Journal of Power Sources 233 (2013) 139–147

Contents lists available at SciVerse ScienceDirect

Journal of Power Sources

journal homepage: www.elsevier.com/locate/jpowsour

Investigation of the degradation of SnO_2 electrodes for use in Li-ion cells

G. Kilibarda [a,b,*], D.V. Szabó [a], S. Schlabach [a], V. Winkler [a,b], M. Bruns [a], T. Hanemann [a,b]

[a] Karlsruhe Institute of Technology, Institute for Applied Materials, ALU, Georges-Köhler-Allee 102, 79110 Freiburg, Germany
[b] University of Freiburg, Department of Microsystems Engineering, ALU, Georges-Köhler-Allee 102, 79110 Freiburg, Germany

HIGHLIGHTS

- Combination of cyclic voltammetry and long term battery cycling on the same half-cell.
- For the first time, areas under the curves were evaluated and set into relation.
- Amount of Li-ions involved in the process, due to reduction and oxidation.
- Evolution of the SEI during cycling, were carried out with *ex-situ* XPS measurements.

ARTICLE INFO

Article history:
Received 24 October 2012
Received in revised form
9 January 2013
Accepted 12 January 2013
Available online 1 February 2013

Keywords:
SnO_2
Li-ion
Degradation
Cyclic voltammogram
Coulombic efficiency
SEI

ABSTRACT

SnO_2 nanoparticle layers were synthesized as electrodes, assembled in lithium half-cells and tested by combining cyclic voltammetry and long-term cycling behavior, supplemented by XPS- and SEM-investigations. The cycling behavior of SnO_2 shows characteristic features: large difference between discharging and charging capacity for the first cycles, pronounced negative slope, corresponding to huge degradation of specific capacity and a shallower slope after achieving coulombic efficiency around 100%. The areas under the charge and discharge curves of the voltammograms are assumed to be a measure for the amount of oxidation and reduction, respectively. The integrated reduction and oxidation areas are not equal after the first cycle (58:42). The whole reaction of the cycle can be described as partially reversible. Consequently, residuals remain, not contributing to capacity in the next cycle. However, after achieving coulombic efficiency around 100%, the area ratio becomes 50:50. The goal of XPS investigation is to show the evolution of the phases while crossing specific potentials. It was shown that the SEI is appearing for the first time by crossing the potential of 1 V. This SEI is dominated by lithium carbonate but also consists of a complex mixture of different lithium compounds and other decomposition products of the electrolyte.

1. Introduction

Nowadays, energy storage has gained an important role in the everyday life. It is a common place to use portable instruments (mobile phones, notebooks, etc.) which are dependent on reliable energy storage equipment. Additionally, the automotive industry searches increasingly for environmentally friendly driving technology, in which electric motors and their batteries are expected to be promising alternatives. In this context, Li-ion batteries are proven to be useful [1].

Graphite anodes are currently state of the art in Li-ion cells. Graphite is an intercalation material which has only little expansion of less than 10% during the cycling. Therefore, the capacity in cycling experiments is nearly constant at 372 mA h g^{-1}. In contrast conversion materials like SnO_2 form alloys with lithium during charging. In this material up to 4.4 Li-ions can be stored ($Li_{22}Sn_5$) [2,3] which results in a theoretical capacity of 782 mA h g^{-1}. The challenge is to keep this capacity constant, because SnO_2 suffers under a huge volume change of around 300% which occurs during cycling [4–7]. Therefore cracks arise all too often, accompanied by a loss of active material.

The cycling behavior of SnO_2 shows characteristic features nearly independent of the particle synthesis or particle morphology. This is obvious by comparing the literature data dealing with several types of SnO_2 electrodes made from SnO_2 nanoparticles, and having a complete different synthesis history [8–12]. Even electrodes containing SnO_2-nanospheres [13], SnO_2-nanowires [14], or SnO_2-nanotubes [15] show a very similar cycling behavior corresponding to the cycling behavior found previously in our

* Corresponding author. KIT, Hermann-von-Helmholtz-Platz 1, 76344 Eggenstein-Leopoldshafen, Germany. Tel.: +49 721 608 23702.
E-mail address: goran.kilibarda@kit.edu (G. Kilibarda).

0378-7753/$ – see front matter © 2013 Elsevier B.V. All rights reserved.
http://dx.doi.org/10.1016/j.jpowsour.2013.01.099

material [16]. Fig. 1 shows exemplarily such a cycling curve, exhibiting the following three relevant features.

- The first observation is a large difference between discharging and charging capacity for the first cycles, representing an irreversible capacity loss.
- Second, in this region a pronounced negative slope, corresponding to huge degradation of specific capacity, is observed.
- However, achieving a coulombic efficiency (CE) of about 100% the slope becomes shallower.

We believe that there are different mechanisms of degradation overlapped in the beginning of cycling, but, after achieving a CE of around 100% some of the mechanisms are not active anymore. This behavior seems to be independent of material synthesis and particle morphology and could be stated as a general rule of degradation. A detailed explanation of these phenomena, to our best knowledge, was not proposed, yet. Therefore, systematic studies, including a dedicated switching between cyclic voltammetry and long term cycling at relevant points using one cell, a detailed evaluation of the cyclic voltammograms, as well as *ex-situ* X-ray photoelectron spectroscopy (XPS) studies of the solid electrolyte interface (SEI) formation at different stages of the cyclic voltammetry and scanning electron microscopy (SEM) after cycling are presented in this paper.

2. Experimental

2.1. Material synthesis and cell assembly

The Karlsruhe microwave-plasma-process was used for the synthesis of SnO_2-nanoparticle layer based electrodes without conventional slurry formation. This process is a gas phase reaction method for the synthesis of nanoparticles [17]. Water free tetra-*n*-butyltin, $Sn(C_4H_9)_4$ (ABCR, Karlsruhe, Germany), is used as precursor for the SnO_2 nanoparticles with a feeding rate of 5 ml h^{-1}. A mixture of 80 vol% Ar + 20 vol% O_2 with a gas flow rate of 5 l min^{-1} was used as reaction gas. The power of the microwave was set to 600 W. These synthesis parameters have been selected, so that a SnO_2 nanoparticle layer thickness of around 2 μm was yielded in all cases. Furthermore, these special conditions enabled the synthesis of SnO_2 nanoparticles, *in-situ* coated with hydrocarbons, C_xH_y, stemming from the organometallic precursor and adsorbed on the nanoparticles surface, necessary for electrical conductivity.

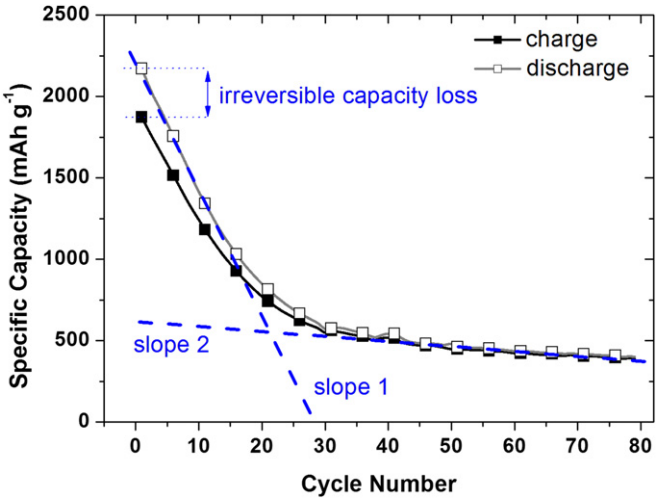

Fig. 1. Typical charge and discharge capacities of a SnO_2 nanoparticle layer electrode. For the first cycles an irreversible capacity loss can be observed. In parallel, a steep slope (1) can be observed until CE reaches 100% and a shallow slope (2) describes the cycling behavior after CE reaches 100%.

The resulting nanoparticles from the process were deposited *in-situ* as porous films on 300 °C preheated Ni-substrates according to the method described in previous studies [16,18,19]. These films were dried in a vacuum oven (Vakucenter VC20, Salvis-Lab, Rotkreuz, Germany) for 2 h at 140 °C.

Altogether six anodes were prepared similarly. One of these anodes was used as reference material without assembling, or cycling. This sample is referred to as pristine. With the other five anodes Swagelok-type half-cells were assembled in an argon-filled Unilab glove box (MBraun, Garching, Germany). The electrodes, consisting only of the *in situ* deposited SnO_2 nanoparticle films, were assembled without any additional carbon black or binder. A glass fiber (Whatman) was used as a separator. Lithium foil (Alfa Aeser, Ward Hill, USA) was used as the counter and reference electrodes. The electrolyte consisted of a solution of 1 M $LiPF_6$ in ethylene carbonate (EC) and dimethyl carbonate (DMC) (50:50) obtained from Merck (LP 30, Merck, Darmstadt, Germany). One of those cells was used for the electrochemical characterization (Section 2.2) and the four remaining cells for the investigation of the SEI formation (Section 2.3). All cells were left for 24 h after assembling to ensure that the electrode is completely wetted with electrolyte.

2.2. Electrochemical characterization

Electrochemical characterization was done using one representative Swagelok half-cell by combining two standard methods. The half-cell was switched between cyclic voltammetry and long term battery cycling, to gain information about oxidation and reduction reactions as well as information about specific capacity with cycling. Therefore, the first three cycles were investigated by cyclic voltammetry, followed by measurements in the battery cycler. After reaching a CE of around 100% in cycling, again three cycles of cyclic voltammetry were performed, followed by measurements in the battery cycler until the 30th cycle. This combination of methods allows characterizing electrochemical processes in one cell. Additionally, a reference measurement of a Swagelok-half-cell using the bare current collector (Ni, without any particle film) was performed by cyclic voltammetry.

Cyclic voltammetry was carried out using an IVIUMSTAT (Ivium-Technologies, Eindhoven, Netherlands) with a measured current resolution and accuracy of ±0.2%. The voltage range was set in the range from 0.1 to 2.5 V (vs. Li^+/Li) by a voltage rate of 0.1 mV s^{-1}. The starting point was at a potential of about 2.5 V of the discharging process. The turn over point at 0.1 V has been chosen to avoid a possible lithium plating occurring at 0 V, which is described especially by using Li-metal as counter electrode [20]. Battery cycling was done using a lithium cell cycler (LICCY, developed at Karlsruhe Institute of Technology, Institute for Data Processing and Electronics) in the voltage range of 0.1–2.8 V (vs. Li^+/Li) at a constant current density of 40 mA g^{-1}.

In the cyclic voltammogram the areas under the charge and discharge curves, respectively, are assumed to be a measure for the amount of oxidation and reduction. For the first time, areas under the curves were evaluated and set into relation, to obtain information about the ratio of reduction and oxidation and the amount of Li-ions involved in the process.

2.3. Investigation of SEI formation

To characterize the evolution of the SEI during the discharge/charge process, *ex-situ* X-ray photoelectron spectroscopy (XPS) measurements were carried out at relevant cycling steps. Fig. 2 shows exemplarily a typical cycling profile of the first cycle,

measured by cyclic voltammetry (a) and the typical voltage profile measured by long term cycling measurements (b) of a SnO_2-nanoparticle layer electrode. The relevant reactions (I–IV) are based on current literature data [14,21,22] and the corresponding voltage steps show where electrodes were investigated (1–4):

Peak I (around 0.9 V, discharge): reduction of SnO_2 to Sn^0 combined with the formation of Li_2O following the reaction $SnO_2 + xLi^+ + xe^- \rightarrow Sn + Li_2O$ and additional reduction of the electrolyte combined with SEI formation.
Peak II (around 0.2 V, discharge): alloying of Li_xSn following the reaction

$$Sn + Li^+ + x^- \rightarrow Li_xSn.$$

Peak III (around 0.5 V, charge): reaction corresponding to Peak II, dealloying of Li_xSn.
Peak IV (around 1.2 V, charge): reaction corresponding to Peak I.

The samples 1–4 are representing four anodes assembled under identical conditions. They were (partly) treated by cyclic voltammetry, and the measurement was stopped at dedicated stages of discharge/charge during the first galvanostatic cycle (points 1–4 in Fig. 2) starting with discharge at 2.5 V. The first half-cell was cycled till 1.9 V, the point just before the reduction of SnO_2 is expected to start (peak I). The second half-cell was cycled till 0.65 V, the point after the SEI-formation is expected to start (peak I), but before alloy formation of Li_xSn begins (peak II). The third half-cell was cycled till 0.1 V in the discharging process, just before dealloying of Li_xSn begins (peak III) and the fourth half-cell was cycled till 2.8 V in the following charging process including the oxidation of Sn to Sn^{y+} (Peak IV). The (partly) cycled half-cells were disassembled in the glove box and the electrodes were washed in a dimethyl carbonate solution. The transport of the disassembled electrodes to the XPS equipment was made in a vacuum-tight transfer box, so the samples did not enter the atmosphere.

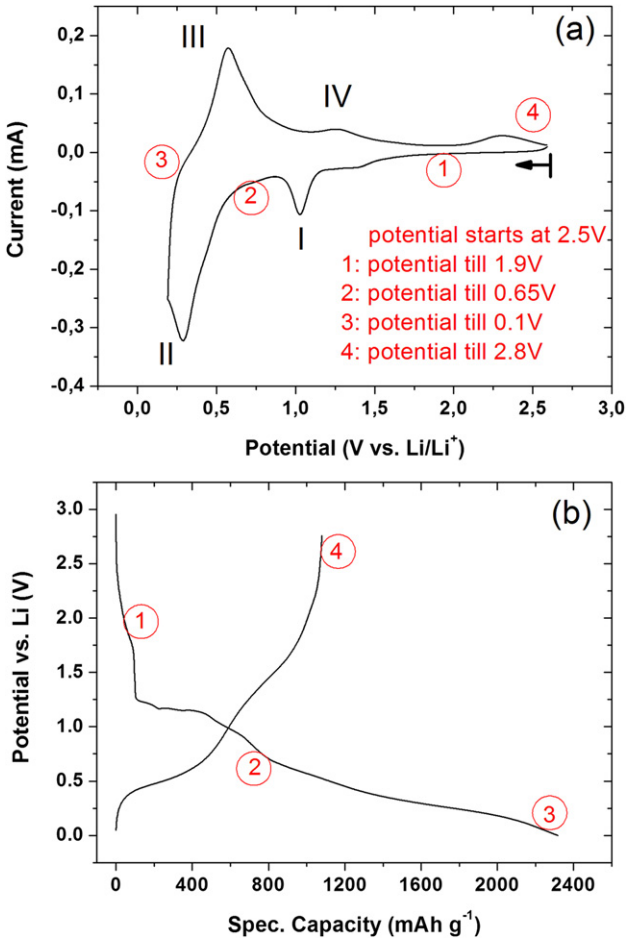

Fig. 2. Typical cyclic voltammogram (a) and voltage profile (b), showing the relevant reactions (I–VI) during cycling and the potential, where *ex-situ* XPS samples were taken (samples 1–4).

The XPS measurements were performed using a K-Alpha XPS spectrometer (ThermoFisher Scientific, East Grinstead, UK). Data acquisition and processing using the Thermo Avantage software is described elsewhere [23]. All samples were analyzed using a microfocused, monochromated Al K_α X-ray source (30–400 μm spot size). The K-Alpha charge compensation system was employed during analysis, using electrons of 8 eV energy and low-energy argon ions to prevent any localized charge build-up. The spectra were fitted with one or more Voigt profiles (binding energy uncertainty: +/−0.2 eV). The analyzer transmission function, Scofield sensitivity factors [24], and effective attenuation lengths (EALs) for photoelectrons were applied for quantification. EALs were calculated using the standard TPP-2M formalism [25]. All spectra were referenced to the C 1s peak of hydrocarbon at 285.0 eV binding energy controlled by means of the well-known photoelectron peaks of metallic Cu, Ag, and Au, respectively.

2.4. Morphology of the nanoparticle layer based electrodes

Selected electrodes were characterized by *ex-situ* scanning electron microscopy (SEM) on a Zeiss Supra55 (Zeiss, Oberkochen, Germany), to obtain information on changes in morphology, occurring during cycling. The electrodes were disassembled in the glove box, and washed in a dimethyl carbonate solution.

3. Results

3.1. General remarks

In our previous work [16,19] X-ray diffraction (XRD) and selected-area small angle electron diffraction (SAED) clearly shows tetragonal cassiterite structure of the SnO_2 nanoparticles. It was also shown, that the nanoparticles form mechanical stable porous layers of columnar structure with thicknesses up to 5 μm, proven by SEM images. Accompanying transmission electron microscopy (TEM) investigations of the SnO_2 nanoparticles made from $Sn(C_4H_9)_4$ using a microwave power of 600 W reveal spherical and crystalline particles with a particle size below 5 nm and a coeval narrow particle size distribution. Furthermore, we know, that this material contains approximately 0.5 wt% of residual water [16], and around 6 wt% of organic hydrocarbons, C_xH_y. These statements are also valid for the material investigated in this study.

3.2. Electrochemical characterization

Cyclic voltammetry of the first three cycles as the first part of the combined characterization is presented in Fig. 3. In agreement with the literature data [21,26] the voltammetry shows the first reduction peak around 0.9 V attributed to Sn and Li_2O formation, described by reaction

$$SnO_2 + xLi^+ + xe^- \underset{OX}{\overset{RED}{\rightleftharpoons}} Sn + Li_2O \quad (1)$$

Here the reduction of SnO_2 to Sn^0 occurs. If an electrode contains an oxide that is less stable than lithium oxide, there will be

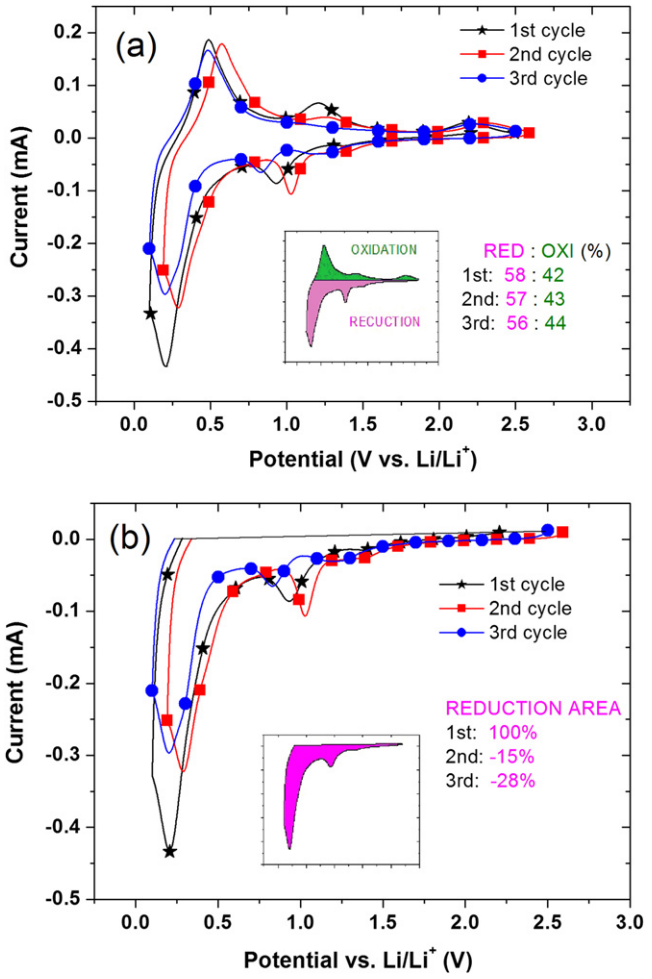

Fig. 3. (a) First three complete cycles measured by cyclic voltammetry at a voltage rate of 0.1 V s^{-1} and the corresponding ratios of the integrated reduction areas (RED) to the oxidation areas (OX). The measured current resolution and accuracy is about ±0.2%, so that the error bar is smaller than the line symbols used. Therefore, the uncertainty of the integrated areas is almost negligible. (b) Decreasing of reduction areas within the first three cycles in relation to the 1st cycle. Symbols are representing only a few of the measured data points to distinguish between the cycles.

a thermodynamic driving force for a displacement reaction in which Li_2O will be formed at the expense of the prior oxide. Hence, a certain amount of Li^+ is consumed in this first forming step. Additionally, the reduction of the electrolyte is also expected at a voltage of around 0.9 V. This reduction can be assigned to the SEI formation and to additional reduction of another organic and inorganic additives from the electrolyte, forming Li–R (lithium and organic residual) [27]. The second cycle shows also the same peak indicating repeating Li_2O, SEI and Li–R formation. One reason might be the cracking of the particle layer; during lithiation and delithiation [4,7,28,29] some parts of this film may break off, as shown in Fig. 4. Whenever fresh surface of active material gets into contact with the electrolyte, new SEI formation takes place [14,30–32] as long as required additives in the electrolyte are not completely consumed. In parallel, reaction (1) will take place.

The most intensive reduction peaks are observed at a voltage around 0.2 V. Here, Sn forms alloys with Li^+ as described by the following reaction:

$$Sn + xLi^+ + xe^- \underset{OX}{\overset{RED}{\rightleftharpoons}} Li_xSn \qquad (2)$$

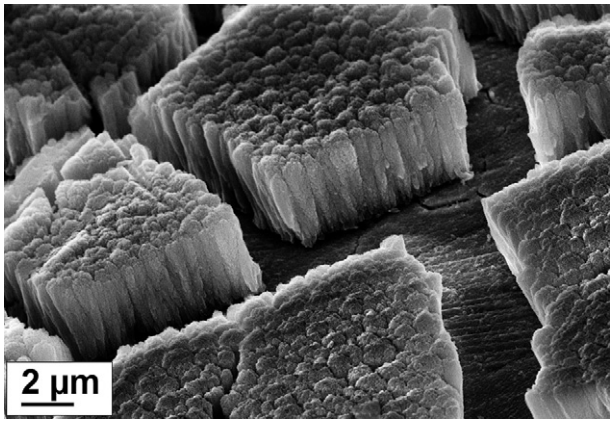

Fig. 4. *Ex-situ* SEM image of a SnO_2-nanoparticle electrode after the first cycle. The building of new, fresh surface area, due to the large volumetric changes accompanied by film break off, is evident from this image.

During charging the corresponding oxidation peaks around 0.5 V (dealloying of Li_xSn), around 1.2 V (oxidation of Sn^0 to SnO_y [21,22,33–37], SEI is assumed to be irreversible) and around 2.2 V (oxidation due to possible reactions of Li and Ni, which was verified by executing a reference measurement) are observed. It is generally accepted, especially in theoretical based literature [2], that reaction (1) is irreversible. Hence, the Li_2O formation is expected to consume Li^+-ions only in the first reduction process and is ascribed to be responsible for the first charge and discharge mismatch. However, the peak at 1.2 V during charging is interpreted as a partial reversibility of reaction (1) and is frequently described in experimental based literature [21,22,33–37]. Considering to this partial reversibility (including Li_2O), the SEI, which acts irreversible, seems to be more responsible for the mismatch in the first cycles.

It should be pointed out, that during the first three cycles the intensities of the integrated oxidation peaks are always smaller than those of the integrated reduction peaks (Fig. 3a). Charging and discharging processes are not in equilibrium. This phenomenon is called partially-reversible. Consequently, the integrated reduction and oxidation areas are not in equilibrium (Table 1), too. Also, both areas are decreasing from cycle #1 to cycle #3 resulting in a decrease of the corresponding number of Li^+-ions. Comparing the integrated areas of the reduction peaks, a decrease of −15% for the second and of −28% for the third cycle compared to the first one can be observed (Fig. 3b). In relation to the decrease of the integrated reduction areas the integrated oxidation areas decrease less pronounced (−7% in the second and −15% in the third, related to the first cycle). As a consequence, the ratio of the integrated reduction areas to the integrated oxidation areas decreases from cycle #1 to cycle #3, too. The results are summarized in Table 1.

When starting the measurements in the long term battery cycler, differences between discharge and charge capacities are still pronounced. The specific capacity is diminishing from cycle to cycle, and the difference between discharge and charge capacities is

Table 1
Relative integrated areas of reduction and oxidation for each cycle and the corresponding number of Li-ions involved in this process.

Cycle #	Reduction area (%)	Oxidation area (%)	Li^+-ions in reduction area	Li^+-ions in oxidation area
1	58	42	11.7	5.5
2	57	43	6.1	5.4
3	56	44	5.9	5.2
13–15	50	50	1.1	1.1

also decreasing. The CE of around 100% is reached in the 12th cycle. This is shown in Fig. 5.

The subsequent cyclovoltammograms (Fig. 6) show that the current is lower by several orders of magnitude, compared to the first three cycles (Fig. 4). Reduction peaks around 1.2 V, and 0.2 V as well as oxidation peaks around 0.5 V, 1.6 V, and 2.2 V are present. It is assumed that the SEI-formation no longer takes place, as no reduction peak is observed immediately by crossing 1 V. Here, the reduction in the electrolyte used to form new SEI probably is complete, as the common additives in the electrolyte are expected to be consumed.

The ratio of the integrated reduction to oxidation areas is now in equilibrium. Nevertheless, both areas are still decreasing with increasing cycle number, as it is shown exemplarily in Fig. 6b for the discharging process in relation to the 13th cycle.

The final measurements in the battery cycler show that the degradation is becoming significantly lower from cycle to cycle, but, does not disappear completely. The difference between discharge and charge capacities is minimal, as the CE of around 100% is reached (Fig. 5).

3.3. Investigation of SEI-formation

To get deeper insights in the formation of a solid electrolyte interface (SEI) during the electrochemical cycling, *ex-situ* analysis by means of XPS was performed in combination with cycling measurements. XPS was chosen as the most widely used surface analysis technique covering a sampling depth of 5–8 nm to provide both chemical state information and quantitative concentration of the detected elements in a non-destructive manner. In particular several SnO_2 electrodes were analyzed at four specific potentials (Fig. 2) and a pristine SnO_2 electrode as well as Li_2CO_3, LiF and $LiPF_6$ were used as reference samples for binding energy assignments. Based on the literature data we expect the reduction of SnO_2 to Sn at voltages less than 1.2 V and relevant SEI formation at voltages below 0.9 V. The XPS results are summarized in Fig. 7, showing the Li 1s (Fig. 7a), C 1s (Fig. 7b) and the Sn 3d (Fig. 7c) spectra. To illustrate the significant changes in the build-up process of a SEI layer we show a direct comparison of the spectra from sample 1

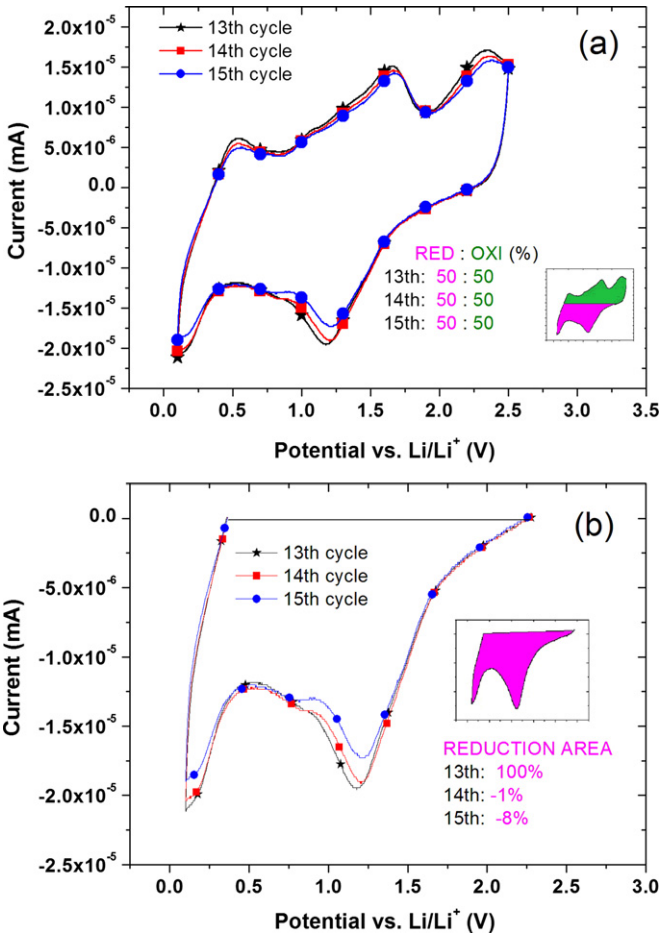

Fig. 6. (a): Three whole cycles by cyclic voltammetry after CE = 100% at a voltage rate of 0.1 V s^{-1} and the ratio of the integrated reduction area to the oxidation area. The measured current resolution and accuracy is about ±0.2%, so that the error bar is smaller than the line symbols used. Therefore, the uncertainty of the integrated areas is almost negligible. (b): Three discharge cycles and their reduction areas. Symbols are representing only a few of the measured data points to distinguish between the cycles.

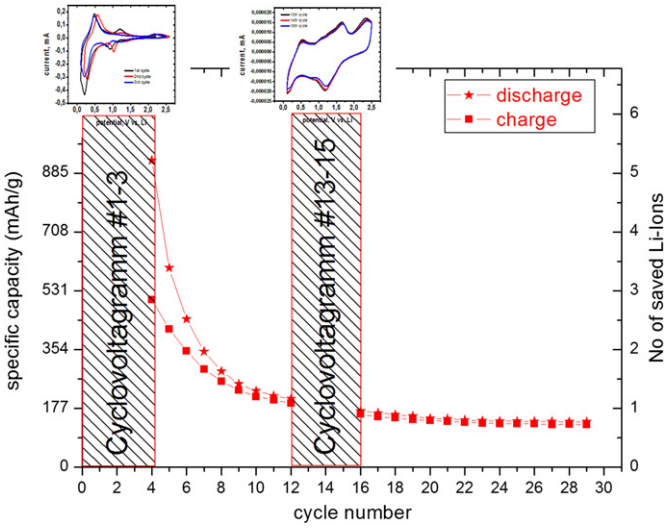

Fig. 5. Result of the cycling treatment: first three cycles with cyclic voltammetry at a voltage rate of 0.1 mV s^{-1}, subsequent long term cycling measurements until a CE of about 100% is reached, using a constant current density of 40 mA g^{-1} and, finally, again three cycles with cyclic voltammetry and final long term cycling measurements until the 30th cycle is reached.

and sample 3. The lithium spectra undoubtedly represent the build-up of a (lithium-rich) SEI layer. The binding energy of the main peak at 55.5 eV fits well to our pure lithium carbonate reference sample (55.4 eV) and the literature data [38]. This carbonate species is also confirmed with a significant peak at a binding energy of 290.2 eV in the carbon spectrum of sample 3 but arises already in sample 2. Another feature of the carbon spectrum is the pronounced peak at 286.5 eV characteristic for carbon species with C–O bonds which could be assigned to various species like alkoxides or poly-carbonates [39,40]. Additionally LiF should be partially included in the SEI layer confirmed with a peak of fluorine at 685.5 eV [40]. This finding can't be clearly supported by evaluating the Li 1s peak. Based on the rather broad and asymmetric Li 1s peak shape we estimated that additionally to Li_2CO_3, the SEI chemistry consists of a complex mixture of various different lithium-rich species originated from the decomposition cascade of the electrolyte. The lack of information about the Li_2O species in the Li 1s spectrum might be due the limited information depth of XPS yielding almost information about the SEI-layer on top. In the case of tin sample 1 shows the Sn $3d_{5/2}$ peak at a binding energy of 487.4 eV identically to the pristine electrode sample which can be assigned to SnO_2 [41]. For sample 3 we can identify a clear visible shift of the main peak toward a lower binding energy of about 486.5 eV which indicates the reduction of Sn^{IV}. However, there is no evidence for the expected

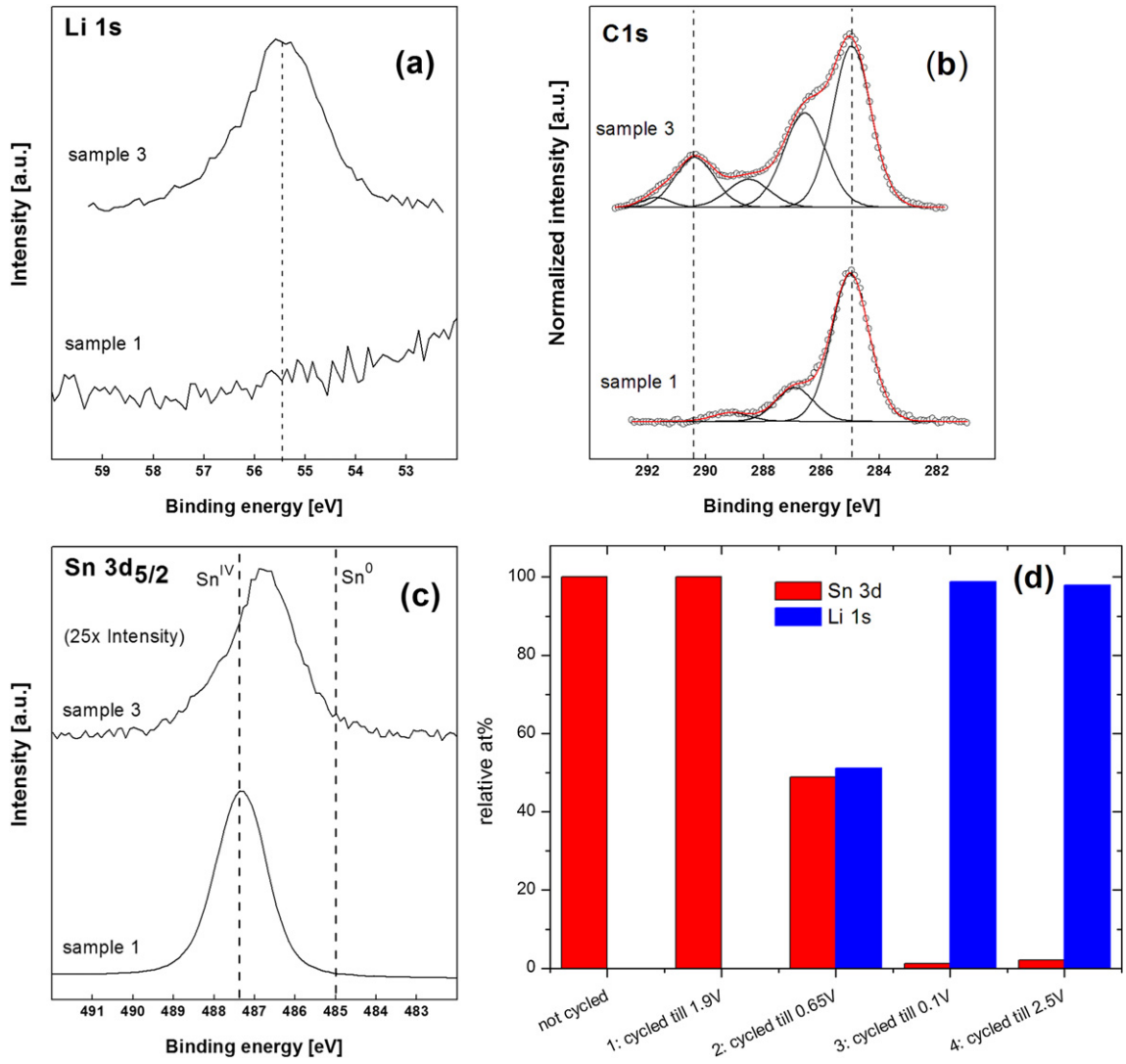

Fig. 7. XPS spectra comparisons between sample 1 and sample 3 ((a) C 1s (b) Li 1s (c) Sn $3d_{5/2}$) and (d) relative atomic ratio of tin and lithium at the investigated potential steps.

Sn^0 species which should appear at a binding energy of about 485.0 eV according to argon-sputter etched tin foil reference sample and literature data [39,40]. This might be due to unavoidable oxygen contamination connected to the executed sample handling and the current XPS setup combined with the high reactivity of tin. Additionally, one should recognize the notably reduced intensity of the Sn 3d peak for sample 3 compared to sample 1, affecting the experimental uncertainty. Nevertheless, this point remains to some extend as an open question. Fig. 7d displays the XPS derived relative atomic ratio of tin and lithium at the investigated potential steps. By increasing cycling (from sample 2 to 4) the atomic percentage of tin is decreasing and that of lithium is increasing. Although there is an estimated error in XPS quantification up to 10% (considering basic assumptions like a flat and homogenous layer system) and an even higher error in our case (spherical particle on the nanoscale with an inhomogeneous SEI-layer on top), a clear trend of the atomic ratios between the characteristic elements tin and lithium can be drawn. This clear trend is a direct proof of the growing SEI layer and therefore the growing of the penetration depth of Li^+ and can't be questioned by any uncertainty in quantification. Because the information depth of XPS is around 5–8 nm and a weak Sn 3d peak is still detectable, the thickness of the SEI layer is in the same magnitude.

4. Discussion

The combination of cyclic voltammetry and long term battery cycling allows a deeper insight into the processes occurring during discharging and charging of an electrode. The results are complemented with XPS and SEM measurements executed on half-cells at significant potential points within cycling.

4.1. Electrochemical characterization

Based on the electrochemical investigation, three significant phenomena are observed

- large difference between discharging and charging capacity for the first cycles, representing an irreversible capacity loss,
- pronounced negative slope, corresponding to huge degradation of specific capacity and
- shallower slope after achieving a coulombic efficiency of about 100%

The observed phenomena are believed to be the result of different processes occurring during discharging and charging. They are explained as follows:

4.1.1. Irreversible capacity loss

Fig. 8 schematically illustrates the cycling behavior during the first discharge and charge processes. As it can be seen, in the discharge process (reduction), there are three reactions which involve Li^+-ions: first is, the formation of Sn and Li_2O, the second is the SEI formation, and third is the formation of Li_xSn ($x = 4.4$). In the charge process (oxidation) only two reactions are involving Li^+-ions: the dealloying of Li_xSn and the reaction (1). The SEI-formation during discharging as a result of the reduction of the electrolyte is assumed to be irreversible and is not participating in the oxidation process.

Furthermore, the alloying–dealloying reaction of Li_xSn seems to be partially-reversible as the number of Li^+-ions involved in the charging process is decreased compared to the preceding discharging (Fig. 4, redox-couple at 0.2 V and 0.5 V, and Table 1).

This unbalanced behavior of discharge and charge (Table 1, ratio of reduction to oxidation not in equilibrium) is repeating for the following cycles resulting in irreversible capacity loss.

4.1.2. Huge degradation for the first cycles

This behavior is attributed to split off (loss of contact) of parts of the active material, due to the large volume changes during discharging and charging, as shown in Fig. 3. This is a continuous process from cycle to cycle, with the largest losses recorded after the first cycle. With diminishing the amount of active material, less Li^+-ions can be stored or pass through the current collector. Therefore, a continuous decrease in capacity can be observed. This decrease in capacity also means a degradation of capacity of the electrode. This mechanism is present during the whole cycling, and frequently described in the literature [15,30,42].

Additionally, the already mentioned partially-reversible process of the alloying and dealloying of Li_xSn contributes to the degradation, too. As can be seen, compared to the charging process there are more Li^+-ions involved during the discharging process. As a consequence, residual Li_xSn alloy remains after charging and in the following discharge process these residuals do not contribute to the capacity. The amount of Sn (SnO_2) acting as active material for the next discharging process is decreasing. The less the amount of this active material, the less the capacity for the following discharging cycles. As already described above, the results given in Table 1 are a measure of this behavior. For the first discharge area a value of 58% is found, for the first charge area one of 42%. The value found for the charging area represents the basic area available for the following discharge process. As a consequence, the following discharge area is less than the previous and the obtainable capacity decreases.

The XPS-measurements showed an increasing SEI thickness with increasing cycling, hence, on a long time scale, the SEI might penetrate into pores of the electrode and in addition may also penetrate into pores of the separator. This may result in a decrease of accessible surface areas due to this continuous growing of the SEI [43]. Additionally, the increasing SEI thickness leads to a rising impedance [43,44], and with this both aspects contribute to the

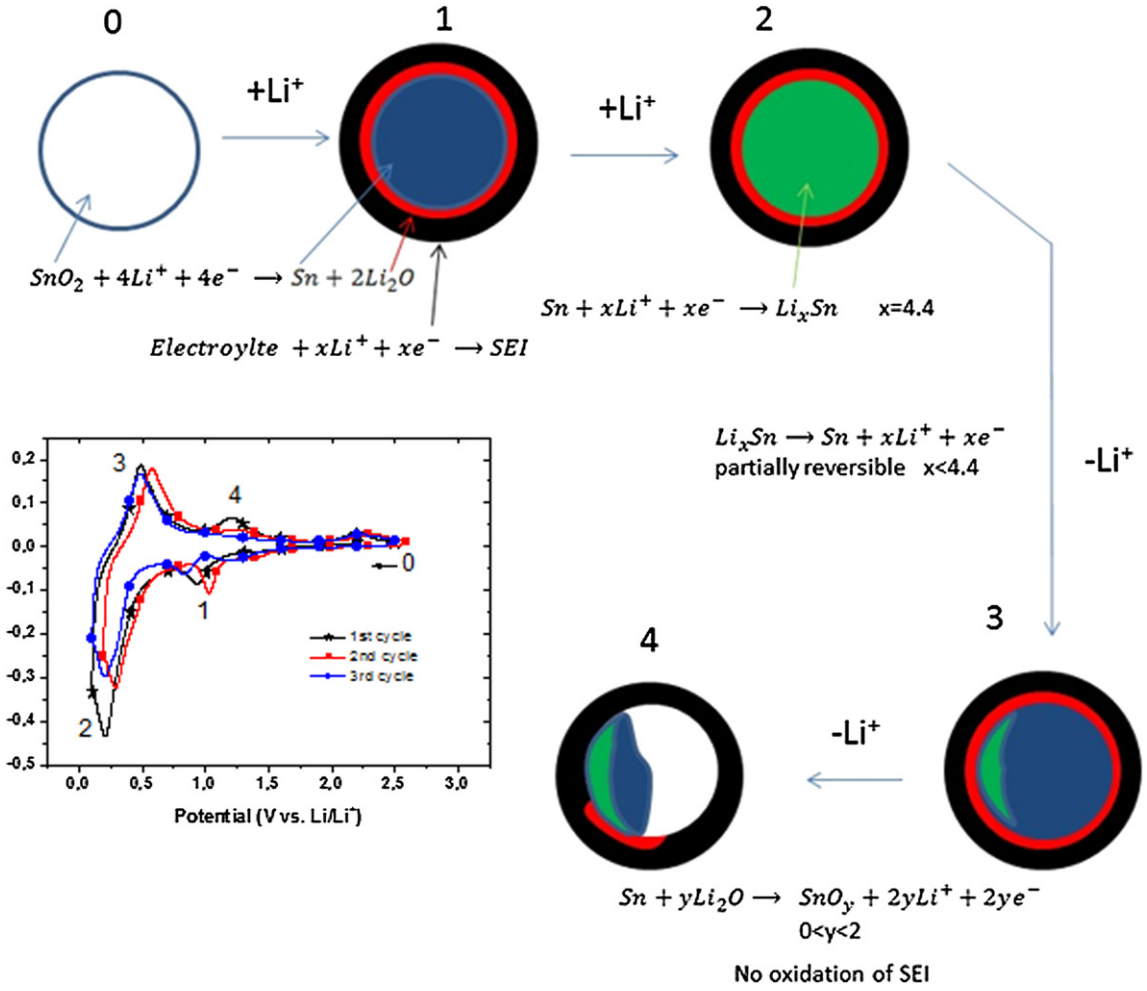

Fig. 8. Schematic illustration of the cycling behavior for the first discharge and first charge processes. For details, see text. It has to be noted that this figure is only schematic and the size, representing amounts of products does not correspond to the real ratio.

capacity available for following cycles. All the described phenomena are inducing a loss of capacity.

4.1.3. Decreasing degradation after achieving CE of around 100%

When the CE of about 100% is achieved, a balance between discharging and charging processes exists. The ratios of the corresponding integrated areas are 50:50, and the numbers of Li^+-ions involved in the discharging and charging processes are the same. As a result, the so far partially reversible reactions seem to achieve a more reversible behavior. Consequently, the trapping of Li^+-ions in residuals is no longer responsible for the degradation of capacity. Lasting degradation is mainly caused by the loss of active material due to the volume changes and the associated loss of contact to the collector.

An additional degradation caused by residual water in the samples, and therefore potential formation of HF in the cell was not discussed in this paper, but cannot be excluded for the whole cycling. The turn over point of 0.1 V should minimize the possibility of lithium plating and in the CV data there is no evidence for this. However, Li-plating is a frequently seen issue and should not be completely neglected.

4.2. Investigation of SEI formation

XPS measurements support the already existing results of the SEI-investigation by cyclic voltammetry. Both methods exhibit a good agreement that the SEI appears for the first time by crossing the 1 V potential. Furthermore, with the XPS analysis the dominant species of the SEI could be assigned to Li_2CO_3, supported by the measurement of pure Li_2CO_3 as reference sample. This finding is also consistent to former literature reports [38,45,46] where mixtures of EC and DMC were used as the electrolyte. In order to ensure the correct detection of the dominant species, all measurements were performed twice and additionally on different places of the electrode. The quantification data are comparable in both cases across the sample. Following the description in the Experimental section, all spectra were fitted using Voigt profiles. The resulting peak binding energies provide the chemical information and atomic concentrations were calculated from the peak intensities corrected for Scofield sensitivity factors, effective attenuation lengths and the analyzer transmission function. Additionally, due to the limited information depth of the XPS the thickness of the SEI could be determined to 5–8 nm justified by a still detectable weak Sn 3d peak of the electrode material.

5. Conclusions

SnO_2 nanoparticle layers were synthesized as electrodes, assembled in lithium half-cells and tested by a combination of cyclic voltammetry and long-term cycling behavior, supplemented by XPS-investigations and SEM-analysis.

Irreversible capacity loss is a consequence of irreversible loss of Li^+-ions. The partially reversibility between reduction and oxidation process (area ratio of 58:42 for the first cycle) shows that more Li^+-ions are introduced by discharging as released by charging. The difference of these Li^+-ions means an irreversible loss of capacity.

The alloying and dealloying process of Li_xSn as the main electrode reaction is found to be partially reversible in the first cycles trapping to some extent Li^+-ions in residuals. As a consequence, the capacity for the next cycle is reduced. The reaction of SnO_2 to Sn and in parallel the formation of Li_2O seems to be partially reversible, too.

When the CE of about 100% is achieved, a balance between discharging and charging processes exists. The ratios of the corresponding integrated oxidation and reduction areas are 50:50, and the associated numbers of Li^+-ions involved in the discharge and charge processes are the same. Thus, the initially partially reversible reaction seems to become reversible. Lasting degradation is mainly caused by the loss of active material due to the volume changes and the associated loss of contact to the collector, which is active during the whole cycling.

Ex-situ XPS measurements were carried out at relevant steps of the cycling process to investigate the formation of the SEI. The SEI chemistry is dominated by the lithium carbonate (Li_2CO_3) but also consists of a complex mixture of different lithium compounds and other decomposition products of the electrolyte. This SEI-film increases within the first cycles. With this, the penetration resistance for Li^+-ions is always getting higher and some Li^+-ions could be retained. Additionally, the increasing SEI thickness may result also in a decrease of accessible surface areas. The results show that the degradation is a result of different processes occurring during charging and discharging.

Acknowledgments

The authors acknowledge financial support by the German Ministry for Education and Research, project "Battery Competence Consortium South—Electrochemistry for Electromobility" under contract number 03KP801.

References

[1] T.-H. Kim, J.-S. Park, S.K. Chang, S. Choi, J.H. Ryu, H.-K. Song, Advanced Energy Materials 2 (2012) 860–872.
[2] R.A. Huggins, Solid State Ionics 113–115 (1998) 57–67.
[3] J. Wang, I.D. Raistrick, R.A. Huggins, Journal of The Electrochemical Society 133 (1986) 457–460.
[4] M. Winter, J.O. Besenhard, Electrochimica Acta 45 (1999) 31–50.
[5] J.O. Besenhard, J. Yang, M. Winter, Journal of Power Sources 68 (1997) 87–90.
[6] Y. Wang, J.Y. Lee, The Journal of Physical Chemistry B 108 (2004) 17832–17837.
[7] L.Y. Beaulieu, K.W. Eberman, R.L. Turner, L.J. Krause, J.R. Dahn, Electrochemical and Solid-State Letters 4 (2001) A137–A140.
[8] Y. Fu, R. Ma, Y. Shu, Z. Cao, X. Ma, Materials Letters 63 (2009) 1946–1948.
[9] L.-Y. Jiang, X.-L. Wu, Y.-G. Guo, L.-J. Wan, The Journal of Physical Chemistry C 113 (2009) 14213–14219.
[10] Y. Wang, J.Y. Lee, Journal of Power Sources 144 (2005) 220–225.
[11] X. Wang, X. Cao, L. Bourgeois, H. Guan, S. Chen, Y. Zhong, D.-M. Tang, H. Li, T. Zhai, L. Li, Y. Bando, D. Golberg, Advanced Functional Materials 22 (2012) 2682–2690.
[12] V. Subramanian, K.I. Gnanasekar, B. Rambabu, Solid State Ionics 175 (2004) 181–184.
[13] Z. Wen, F. Zheng, K. Liu, Materials Letters 68 (2012) 469–471.
[14] M.-S. Park, G.-X. Wang, Y.-M. Kang, D. Wexler, S.-X. Dou, H.-K. Liu, Angewandte Chemie International Edition 46 (2007) 750–753.
[15] M.-S. Park, Y.-M. Kang, G.-X. Wang, S.-X. Dou, H.-K. Liu, Advanced Functional Materials 18 (2008) 455–461.
[16] D.V. Szabó, G. Kilibarda, S. Schlabach, V. Trouillet, M. Bruns, Journal of Materials Science 47 (2012) 4383–4391.
[17] D. Vollath, D. Szabó, Journal of Nanoparticle Research 8 (2006) 417–428.
[18] B. Schumacher, R. Ochs, H. Trösse, S. Schlabach, M. Bruns, D.V. Szabó, J. Haußelt, Plasma Processes and Polymers 4 (2007) S865–S870.
[19] R. Ochs, D.V. Szabó, S. Schlabach, S. Becker, S. Indris, Physica Status Solidi A 208 (2011) 471–473.
[20] W. Fredriksson, K. Edström, Electrochimica Acta 79 (2012) 82–94.
[21] H. Liu, D. Long, X. Liu, W. Qiao, L. Zhan, L. Ling, Electrochimica Acta 54 (2009) 5782–5788.
[22] M. Mohamedi, S.-J. Lee, D. Takahashi, M. Nishizawa, T. Itoh, I. Uchida, Electrochimica Acta 46 (2001) 1161–1168.
[23] K.L. Parry, A.G. Shard, R.D. Short, R.G. White, J.D. Whittle, A. Wright, Surface and Interface Analysis 38 (2006) 1497–1504.
[24] J.H. Scofield, Journal of Electron Spectroscopy and Related Phenomena 8 (1976) 129–137.
[25] S. Tanuma, C.J. Powell, D.R. Penn, Surface and Interface Analysis 21 (1994) 165–176.
[26] M. Marcinek, L.J. Hardwick, T.J. Richardson, X. Song, R. Kostecki, Journal of Power Sources 173 (2007) 965–971.
[27] C. Alexandre, S. Jolanta, in: I. Belharouak (Ed.), Lithium Ion Batteries – New Developments, 2012.
[28] J. Liu, Y. Li, X. Huang, R. Ding, Y. Hu, J. Jiang, L. Liao, Journal of Materials Chemistry 19 (2009) 1859–1864.

[29] J.P. Maranchi, A.F. Hepp, P.N. Kumta, Electrochemical and Solid-State Letters 6 (2003) A198–A201.
[30] M. Wachtler, J.O. Besenhard, M. Winter, Journal of Power Sources 94 (2001) 189–193.
[31] J.-T. Li, S.-R. Chen, X.-Y. Fan, L. Huang, S.-G. Sun, Langmuir 23 (2007) 13174–13180.
[32] I.T. Lucas, E. Pollak, R. Kostecki, Electrochemistry Communications 11 (2009) 2157–2160.
[33] X.W. Lou, J.S. Chen, P. Chen, L.A. Archer, Chemistry of Materials 21 (2009) 2868–2874.
[34] J. Yao, X. Shen, B. Wang, H. Liu, G. Wang, Electrochemistry Communications 11 (2009) 1849–1852.
[35] R. Liu, N. Li, D. Li, G. Xia, Y. Zhu, S. Yu, C. Wang, Materials Letters 73 (2012) 1–3.
[36] S. Han, B. Jang, T. Kim, S.M. Oh, T. Hyeon, Advanced Functional Materials 15 (2005) 1845–1850.
[37] R. Demir-Cakan, Y.-S. Hu, M. Antonietti, J. Maier, M.-M. Titirici, Chemistry of Materials 20 (2008) 1227–1229.
[38] S. Leroy, H. Martinez, R. Dedryvère, D. Lemordant, D. Gonbeau, Applied Surface Science 253 (2007) 4895–4905.
[39] J.-T. Li, J. Świątowska, V. Maurice, A. Seyeux, L. Huang, S.-G. Sun, P. Marcus, The Journal of Physical Chemistry C 115 (2011) 7012–7018.
[40] S. Naille, R. Dedryvère, H. Martinez, S. Leroy, P.E. Lippens, J.C. Jumas, D. Gonbeau, Journal of Power Sources 174 (2007) 1086–1090.
[41] M. Fuchs, D. Breitenstein, M. Fartmann, T. Grehl, S. Kayser, R. Koester, R. Ochs, S. Schlabach, D.V. Szabó, M. Bruns, Surface and Interface Analysis 42 (2010) 1131–1134.
[42] Y. Wang, J.Y. Lee, H.C. Zeng, Chemistry of Materials 17 (2005) 3899–3903.
[43] J. Vetter, P. Novák, M.R. Wagner, C. Veit, K.C. Möller, J.O. Besenhard, M. Winter, M. Wohlfahrt-Mehrens, C. Vogler, A. Hammouche, Journal of Power Sources 147 (2005) 269–281.
[44] P. Ramadass, B. Haran, R. White, B.N. Popov, Journal of Power Sources 112 (2002) 606–613.
[45] H. Li, X. Huang, L. Chen, Electrochemical and Solid-State Letters 1 (1998) 241–243.
[46] X.W. Guo, X.P. Fang, Y. Sun, L.Y. Shen, Z.X. Wang, L.Q. Chen, Journal of Power Sources 226 (2013) 75–81.